

The cytokinetic midbody mediates asymmetric fate specification at mitotic exit during neural stem cell division

Bryce LaFoya, Rhiannon R Penkert, and Kenneth E. Prehoda¹

Institute of Molecular Biology
Department of Chemistry and Biochemistry
1229 University of Oregon
Eugene, OR 97403

¹Corresponding author: prehoda@uoregon.edu

1 Summary

2 Asymmetric cell division (ACD) is a broadly used mechanism for generating cellular diversity. Molecules
3 known as fate determinants are segregated during ACD to generate distinct sibling cell fates, but
4 determinants should not be activated until fate can be specified asymmetrically. Determinants could be
5 activated after cell division but many animal cells complete division long after mitosis ends, raising the
6 question of how activation could occur at mitotic exit taking advantage of the unique state plasticity at
7 this time point. Here we show that the midbody, a microtubule-rich structure that forms in the
8 intercellular bridge connecting nascent siblings, mediates fate determinant activation at mitotic exit in
9 neural stem cells (NSCs) of the *Drosophila* larval brain. The fate determinants Prospero (Pros) and Brain
10 tumor (Brat) are sequestered at the NSC membrane at metaphase but are released immediately
11 following nuclear division when the midbody forms, well before cell division completes. The midbody
12 isolates nascent sibling cytoplasm, allowing determinant release from the membrane via the cell cycle
13 phosphatase String, without influencing the fate of the incorrect sibling. Our results identify the
14 midbody as a key facilitator of ACD that allows asymmetric fate determinant activation to be initiated
15 before division.

16

17 Introduction

18 Asymmetric cell division (ACD) is a fundamental mechanism for generating cellular diversity, employed
19 by organisms across the tree of life¹⁻⁶. During development and homeostasis, ACDs generate
20 specialized cell types by producing sibling cells that assume distinct fates. Factors known as fate
21 determinants are central players in ACDs as they maintain or alter sibling cell state. The segregation of
22 fate determinants into the siblings, through determinant polarization and division plane alignment, is
23 the central feature of current ACD models². However, segregation may not fully capture the essential
24 features of ACD. Transcription factor fate determinant activation is an example of an essential ACD
25 process that is not explained by segregation. Many fate determinants are transcription factors that are
26 polarized on the membrane during division to facilitate segregation but must be released from the
27 membrane and imported into the nucleus to regulate gene activity. This example highlights a critical
28 knowledge gap in our understanding of ACD: how fate determinants are activated to achieve
29 asymmetric sibling cell states.

30 The model for intrinsic ACDs (those that are cell autonomous) has been well-established for at least 30
31 years¹ but doesn't account for fate determinant regulation. In the ACD standard model, segregation of

32 fate determinants is the central feature responsible for the distinct fates of the resulting sibling cells.
33 Fate determinants are segregated by their polarization during the division process and alignment of the
34 polarity and division axes, causing their specific deposition into only one sibling^{1,2,4,5,7}. While
35 segregation determines which sibling receives a determinant, it does not specify whether the
36 determinant is active in the sibling. In fact, for reasons we outline here, fate determinant activity
37 transitions are likely general features of ACD that are hidden within the current segregation-focused
38 standard model (Fig. 1A). These transitions are likely to be highly regulated since the activity of
39 determinants before sibling separation could cause the asymmetry of the division to be lost. The fate
40 determinant Prospero (Pros in *Drosophila*; Prox1 in mammals) functions in asymmetrically dividing
41 *Drosophila* neural stem cells (NSCs; aka neuroblasts) and illustrates this problem⁸⁻¹¹. Pros is a
42 transcription factor that is critical for specifying the fate of the differentiating sibling cell (NP; neural
43 progenitor) following an NSC division (the other sibling remains an NSC; Fig. 1A). During division, Pros
44 is polarized to the basal plasma membrane but eventually becomes nuclear in the NP sibling where it
45 can bind chromatin and alter gene expression^{8,9}. Thus, Pros' membrane binding plays a dual role –
46 along with the commonly understood function to facilitate segregation, it also inhibits Pros'
47 transcription factor activity by sequestering it away from the nucleus. Pros must ultimately be released
48 from the membrane, but only when doing so would allow the NP fate to be specified without corrupting
49 the fate of the NSC sibling. Understanding when and how Pros is activated is therefore a critical aspect
50 of the NSC ACD mechanism, but little is known about this essential transition. In terms of the standard
51 ACD model, the Pros example highlights what has been an implicit but essential feature of the model –
52 that fate determinants are inactive during the polarization step but become activated at some later
53 point.

54 Cell fate transitions have been proposed to be coupled to cell division^{6,12,13} suggesting that fate
55 determinant activation could be linked to the final step of division, abscission. Division (i.e. cytokinesis)
56 is a seemingly natural boundary for determinant activation and asymmetric fate specification because
57 determinants cannot pass between siblings following abscission. On the other hand, transcriptional
58 programs that control cellular identity can be rapidly set at mitotic exit because of chromosome
59 decompaction and epigenetic changes¹⁴⁻¹⁷, including global reactivation of transcription¹⁸. However,
60 many animal cells undergo abscission long after mitosis with the nascent sibling cells remaining
61 connected by an intercellular bridge for an extended period in G1 phase¹⁹⁻²¹. Thus, the delay between
62 the end of mitosis and cell division represents a paradox – initiating fate determinant activation after

63 abscission would safely allow for asymmetric fate specification but with the ideal window for altering
64 cell fate potentially having passed. We sought to resolve this paradox and determine when fate
65 determinant activation is initiated by examining determinant and cell cycle dynamics in the
66 asymmetrically dividing NSCs of the *Drosophila* larval brain.

67 Results

68 Fate determinant activation begins before cell division completes

69 The fate determinant Pros localizes to the NSC basal membrane at metaphase^{8,9}. Pros is ultimately
70 released from the membrane so that it can enter the nucleus of the NP sibling. A previous study
71 examined Pros nuclear import relative to early furrowing²² but the timing of release and nuclear entry
72 relative to the late steps of cytokinesis has not been known. We used high speed, super-resolution live
73 imaging NSCs (Fig. 1B) expressing Pros-GFP and the membrane marker PLC δ -PH-mCherry, to
74 determine when Pros membrane release occurs relative to cytokinesis. Pros was initially targeted to the
75 basal membrane several minutes before furrow ingression began where it remained until late
76 cytokinesis (Fig. 1C,D and Video 1). Surprisingly, Pros was released from the membrane while the
77 nascent siblings remained connected by the intercellular bridge, a thin, pore-forming tube of plasma
78 membrane. We measured an average cytokinetic pore diameter of approximately 0.6 μ m when Pros
79 was released from the membrane ($0.59 \pm 0.07 \mu$ m; 1 SD, n = 10 divisions from distinct NSCs). Pros
80 rapidly entered the nucleus after release without any significant cytoplasmic accumulation. Pore
81 constriction in late cytokinesis is slow in the dividing NSC²³ (Fig. 1E), leading to a substantial delay
82 between Pros membrane release and the pore reaching the diameter at which abscission can take place
83 (approximately 200 nm)²⁴. We also observed large tubules or sheets of plasma membrane forming near
84 the pore during this phase (Fig. 1C and Video 1), consistent with a previous report²⁵. We conclude that
85 the initial Pros activating step – its release from the membrane – and its subsequent entry into the NP
86 nucleus, occur well before cell division completes.

87 The timing of Pros translocation from the membrane to the nascent NP nucleus before division
88 prompted us to examine fate determinant activation in the nascent NSC. Deadpan (Dpn) is a
89 transcription factor that specifies NSC fate²⁶ and localizes specifically to the NSC nucleus. We found
90 that Dpn entered the nascent NSC nucleus before division completed (Fig. 1F,G; pore diameter $0.97 \pm$
91 0.38μ m; 1 SD, n = 3 divisions from distinct NSCs), on average slightly earlier than Pros entered the
92 nascent NP nucleus. Thus, asymmetric fate specification is initiated in both the nascent NSC and NP
93 siblings before cell division completes (Fig. 1H).

94 Asymmetric fate specification likely occurs after nuclear division (i.e. mitosis) completes, and the rapid
95 entry of Pros into the nascent NP nucleus immediately following membrane release is consistent with
96 this hypothesis. We imaged several markers for the end of mitosis along with the plasma membrane to
97 compare the relative timing of nuclear and cell division. Mitotic chromosomes were decompacted at a
98 pore size of approximately $3 \mu\text{m}$ (3.0 ± 0.7 ; $n = 3$), as assessed by Histone 2A (Fig. 2A,B; Video 2). Nuclei
99 were separated at $1.3 \pm 0.1 \mu\text{m}$ ($n = 3$) pore size according to the nuclear membrane marker Klaroid (Fig.
100 2B,C; Video 2). Finally, an NLS-DsRed fusion was imported into the nascent NSC and NP nuclei at $1.0 \pm$
101 $0.4 \mu\text{m}$ ($n = 3$) pore size (Fig. 2B,D; Video 2). Together, these observations establish a timeline of events
102 that occur during late mitosis and cytokinesis, along with the initiation of asymmetric fate determinant
103 activation (Fig. 2E). Fate determinant activation is initiated immediately following the events of late
104 mitosis, but well before the cytokinetic pore reaches 200 nm and the ESCRT-III machinery can carry out
105 the final step of cytokinesis, the resolution of the plasma membrane or abscission²⁴. The entry of fate
106 determinants into the nucleus before abscission suggests that a mechanism exists that allows
107 asymmetric fate specification to occur while the nascent siblings remain connected.

108 **Nascent sibling cytoplasm is isolated before cell division completes**

109 Fate determinant release into the cytoplasm while the nascent siblings remain connected raises the
110 question of how determinants are prevented from corrupting the fate of the incorrect sibling (e.g. why
111 doesn't Pros enter the nascent NSC cytoplasm and nucleus?). One possibility is that cellular structures
112 besides the plasma membrane prevent fate determinants from escaping their nascent sibling's
113 cytoplasm after membrane release, similar to the function of the bud neck in budding yeast^{27,28}. To test
114 this hypothesis, we examined the dynamics of the fate determinant Brain tumor (Brat). Brat is a
115 translational repressor that functions in the cytoplasm of the NP once it is released from the
116 membrane^{29,30}. We used Brat's cytoplasmic localization to determine whether cytoplasmic exchange
117 occurs between the nascent siblings. Brat was released from the membrane when the cytokinetic pore
118 reached a diameter of approximately $0.7 \mu\text{m}$ (Fig. 3A,B; Video 3), similar to when Pros is released. There
119 was a correspondingly rapid increase in cytoplasmic Brat that was specific to the nascent NP (Fig. 3B).
120 Brat's accumulation in the nascent NP cytoplasm indicates that the pore connecting the nascent
121 siblings impedes Brat transfer into the nascent NSC cytoplasm.

122 **Pre-division fate determinant isolation requires the midbody**

123 The ability of Brat and Pros to influence the fate of the NP sibling depends on their release from the
124 plasma membrane. Our results indicate that the determinant activation that begins with membrane

125 release occurs before cell division has completed. Furthermore, cytoplasmic exchange of the
126 determinants between nascent siblings, which could corrupt the fate of the NSC sibling, is inhibited in
127 late cytokinesis when determinants are released from the membrane. Release begins shortly after the
128 cytokinetic pore reaches 1.5 μm in diameter, when the cytokinetic midbody forms. The midbody is a
129 microtubule-rich structure that is constructed inside the pore formed by the intercellular bridge and
130 facilitates abscission³¹. Furthermore, the midbody can inhibit exchange of proteins between nascent
131 sibling cell cytoplasm before abscission³². We imaged microtubules and a marker of midbody
132 microtubules, Fascetto (Feo; PRC1 in worms and mammals), which binds central spindle microtubules
133 and bundles them during midbody formation, to examine midbody formation in asymmetric NSC
134 divisions and verify that the midbody forms before fate determinant activation begins (Fig. 3C,D; Video
135 3). These data revealed that central spindle microtubules become compacted within the pore
136 connecting the nascent siblings. The microtubules transition from having clear gaps during early
137 furrowing, to a point at which there are no apparent gaps once the pore diameter reached
138 approximately 1.5 μm (Fig. 3C,D; Video 3). Thus, the midbody forms a continuous structure in the pore
139 nearly simultaneously with fate determinant membrane release. These observations are consistent
140 with a potential role for the midbody in fate determinant activation by preventing determinant
141 exchange between nascent siblings (Fig. 3E).

142 To determine if asymmetric fate specification requires cytoplasmic isolation by the midbody, we
143 ablated the midbody shortly after formation and examined whether Brat was retained in the nascent
144 NP cytoplasm. We used a cytoskeleton depolymerization strategy to ablate the midbody. In cultured
145 cells and worm embryos, actin filament or microtubule depolymerization alone is insufficient to disrupt
146 the midbody but their combined action ablate the structure^{32,33}. Consistent with these reports, we
147 found that addition of the actin depolymerizing drug Latrunculin A (LatA) to NSCs shortly before
148 midbody formation caused furrow retraction, whereas depolymerization after formation inhibited
149 further pore constriction while maintaining the connecting bridge (Fig. 4A,B; Video 4). We used
150 Colcemid to depolymerize the midbody microtubules in LatA frozen midbodies and examined the
151 dynamics of cytoplasmic Brat. Unlike in untreated or LatA alone-treated dividing NSCs, where Brat
152 remained restricted to the cytoplasm of the nascent NP, we observed rapid Brat dissipation into the
153 much larger NSC sibling in LatA + Colcemid treated cells (Fig. 4C-E; Video 4). We conclude that the
154 midbody is required to maintain asymmetric distribution of fate determinants during late cytokinesis by
155 acting as a barrier to cytoplasmic exchange between the sibling cells.

156 Initiation of asymmetric fate specification requires midbody formation

157 Our results support a model in which the midbody plays a critical role in ACD by isolating nascent
158 sibling cytoplasm from one another when fate determinants are released from the membrane, thus
159 ensuring the fate of the incorrect sibling is not corrupted. The key role of the midbody in initiating
160 asymmetric fate specification led us to ask if midbody formation could be a prerequisite for
161 determinant membrane release. We tested this hypothesis by following Pros dynamics in NSCs in
162 which midbody formation was inhibited. The microtubule stabilizing factor Fascetto (Feo; aka PRC1) is
163 a key component of the midbody and is recruited to central spindle microtubules through interactions
164 with the kinesin Klp3a (aka KIF4A)^{34,35}. The interaction of Feo with Klp3a is promoted by Aurora B
165 phosphorylation³⁶. We verified that NSC midbody formation could be inhibited by addition of the
166 Aurora B inhibitor Binucleine 2³⁷. Dividing NSCs treated with inhibitor immediately before midbody
167 formation lost Feo signal on the central spindle and failed to form a stable midbody, leading to furrow
168 retraction (Fig. 5A; Video 5). In contrast, cells with recently formed midbodies maintained their furrows
169 following Aurora B inhibition (Fig. 5B,C; Video 5). Nuclei from midbody inhibited NSCs imported a
170 nuclear import marker at the completion of mitosis, indicating that exit from mitosis and subsequent
171 import was not affected in these cells (Fig. 5D; Video 5). We examined Pros dynamics in Aurora B-
172 inhibited NSCs, both before and after midbody formation. Pros release was significantly delayed in cells
173 where midbody formation was inhibited by Aurora B (Fig. 5F,G). However, Pros was released from the
174 membrane normally in Aurora B-inhibited cells that had already formed a midbody (Fig. 5E,G; Video 5).
175 Consistent with the inhibition of membrane release, Pros also failed to enter the nucleus in midbody-
176 inhibited NSCs (Fig. 5H). We also observed a requirement for the midbody for Brat membrane release
177 (Fig. 5I-K). These results suggest that midbody formation is required for initiating asymmetric fate
178 specification through release of fate determinants from the membrane.

179 The cell cycle phosphatase String regulates fate determinant release after midbody formation

180 Our results indicate that the release of fate determinants from the membrane that initiates asymmetric
181 fate specification occurs before cell division completes. Formation of the midbody appears to be a
182 prerequisite for determinant membrane release such that the signals that control release appear to be
183 activated only after the midbody isolates nascent sibling cytoplasm from one another. We sought to
184 identify signaling factors that regulate release of determinants from the membrane post-midbody
185 formation and screened cell cycle inhibitors for their effect on Pros membrane release attempting to
186 identify regulators that promote release without disrupting midbody formation. Addition of an inhibitor

187 of String (Cdc25 in mammals), a cell cycle phosphatase, after the onset of furrowing significantly
188 delayed Pros membrane release without any detectable effect on midbody formation (Fig. 6A,B; Video
189 6). Although Cdc25 has been reported to be degraded near the end of mitosis, we detected signal with
190 an anti-String antibody in NSCs during late cytokinesis (Fig. 6C).

191 Discussion

192 We examined fate determinant dynamics at high temporal resolution and discovered a new function for
193 the cytokinetic midbody in ACD. This function is essential for timely fate determinant activation,
194 highlighting the importance of determinant regulation during ACD. Fate determinants such as Brat and
195 Pros are polarized on the plasma membrane during division as a mechanism for their segregation, but it
196 was not known when they are released from the membrane relative to both nuclear and cell division.
197 We hypothesized that they would not be released until sometime after division to ensure that they do
198 not enter the cytoplasm of the incorrect sibling cell, potentially corrupting its fate. Surprisingly,
199 however, we found that asymmetric fate specification is initiated by fate determinant membrane
200 release long before cell division completes. Determinants are rapidly released after nuclear division,
201 while the nascent sibling cells remain attached by the midbody-containing intercellular bridge. Brat and
202 Pros accumulate in the nascent NP cytoplasm and nucleus, respectively, without exchanging into the
203 nascent NSC, indicating that determinants do not exchange between the siblings. Disrupting the
204 midbody causes Brat to leak out of the nascent NP indicating that the midbody is required to prevent
205 determinant diffusion between the nascent siblings. These results provide a framework for
206 understanding determinant activation and support a key role for the midbody in ACD.

207 The midbody was discovered in the late 19th century by early cell division researchers³⁸ and its highly
208 organized structure suggests an important role in cellular function. Only recently, this was borne out by
209 the discovery that the midbody recruits and positions the abscission machinery once the pore has
210 constricted to a diameter of 200 nm²⁴. Our discovery suggests that the midbody is important at a much
211 earlier timepoint, shortly after it is formed from the compacted central spindle and associated proteins.
212 Midbody-connected siblings can persist well into the following interphase³⁹, forming a temporal
213 window between mitotic and cytokinetic exit. Taking advantage of this period to specify cell state could
214 be important in rapidly proliferating tissues like the developing brain. Thus, the midbody allows
215 asymmetric fate specification to begin immediately following nuclear division, when large-scale
216 transcriptional activity has resumed.

217 The barrier function of the NSC midbody is reminiscent of the bud neck in budding yeast by acting as a
218 diffusion barrier^{27,28}. However, not all midbodies appear to prevent exchange across the intercellular
219 bridge. An early study found that molecules as large as antibodies pass across the bridge formed by
220 dividing HeLa cells⁴⁰. More recently cultured mouse embryonic stem cells have been demonstrated to
221 remain connected by an freely passable intercellular bridge following mitosis, only exiting naïve
222 pluripotency after division³². Other midbodies, besides the NSC's, restrict passage, however. The
223 midbody formed by the first division of the worm zygote prevents exchange³², as does the meiotic
224 midbody formed by mammalian oocytes⁴¹. This diversity suggests that the midbody structure might
225 have the capability to be tuned to inhibit or allow diffusion between nascent siblings.

226 We propose that fate determinant membrane release is part of a highly choreographed sequence of
227 events at the end of mitosis and during late cytokinesis that are centered around the midbody.
228 Midbody formation, characterized by central spindle compaction and straightening of the furrow
229 membrane into the highly cylindrical intercellular bridge, takes place alongside mitotic exit (Figs. 2,3;
230 Videos 2 & 3). The pore constricts from approximately 1.5 μm to 200 nm, the diameter at which
231 abscission can occur, and fate determinants release from the membrane shortly after constriction
232 begins. Our results suggest that the mitotic phosphatase String is required for Pros membrane release
233 after midbody formation. Further work will be required to understand how String activity might be
234 connected to midbody dynamics to ensure that Pros is not released before the cytoplasmic exchange
235 barrier has been established.

236 Figure Legends

237 Figure 1 Asymmetric fate specification is initiated before NSC division completes

238 (A) Uncovering the hidden steps in asymmetric cell division. The standard model (top) focuses on fate
239 determinant segregation through polarization and division plane orientation. The focus on segregation
240 obscures a key element of the model that is likely a general feature, fate determinant regulation
241 (bottom). In this example, the fate determinant is a transcription factor polarized on the plasma
242 membrane during neural stem cell (NSC) division. The transcription factor must be released from the
243 membrane and imported into the nucleus to influence the neural progenitor (NP) sibling state.

244 (B) Imaging NSC asymmetric divisions. Larval *Drosophila* brains explants are cultured and imaged using
245 spinning disk confocal microscopy. NSCs and their progeny are identified through the position in the
246 brain and expression of membrane marker driven by the NSC driver, *Worniu-GAL4*.

247 (C) Dynamics of the fate determinant Prospero (Pros) during the late stages of NSC asymmetric
248 division. Frames from Video 1 are shown with Pros-GFP expressed from its endogenous locus and the
249 plasma membrane marker PLC δ -PH-mCherry (expressed with *Worniu-GAL4* driven UAS; “membrane”)
250 through an optical section containing the cytokinetic pore. Arrowheads point to cortical Pros signal in
251 dividing NSC and nascent NP sibling. Time in minutes relative to the presence of nuclear Pros is shown
252 along with the diameter of the cytokinetic pore in microns. Panels containing both Pros and membrane
253 signal are shown in the third row along with an inset in the fourth row that focuses on the cytokinetic
254 pore and NP sibling. Bottom row shows a schematized representation of the localization within the
255 dividing NSC.

256 (D) Quantification of Pros membrane release. The diameters of the pore connecting nascent siblings
257 when nuclear signal was detected for Pros is shown. Each point represents a distinct NSC division.
258 Abscission, the final step of cytokinesis, does not occur until sometime after the pore reaches 200 nm
259 (grey line).

260 (E) Quantification of cytokinetic pore closure dynamics during NSC ACD. The solid line represents the
261 mean of five distinct NSC divisions and the shaded region represents one standard deviation.

262 (F) Dynamics of asymmetric nuclear Deadpan (Dpn). Frames from Video 1 are shown with Dpn-GFP
263 expressed from its endogenous locus and the plasma membrane marker PLC δ -PH-mCherry (expressed
264 with *Worniu-GAL4* driven UAS) through a section containing the cytokinetic pore. Time in minutes
265 relative to presence of nuclear Dpn is shown along with the diameter of the cytokinetic pore in microns.

266 (G) Quantification of Dpn nuclear import. The diameters of the pore connecting nascent siblings when
267 nuclear signal was detected for Dpn are shown as in (D).

268 (H) Pre-division initiation of asymmetric fate specification. Pros is released from the membrane and
269 enters the nascent NP nucleus without entering the NSC nucleus.

270 Figure 2 A temporal window between mitosis and cytokinesis during NSC ACD

271 (A) Chromatin dynamics during late NSC division focusing on the cytokinetic pore and nascent NP
272 sibling. Frames from Video 2 are shown with PLC δ -PH-GFP (expressed with Worniu-GAL4 driven UAS)
273 and the chromatin marker RFP tagged Histone 2A (His2a-RFP expressed from its endogenous locus)
274 through an optical section containing the cytokinetic pore. Time in minutes relative to the chromosome
275 decompaction is shown along with the diameter of the cytokinetic pore in microns. A schematic
276 representation of the localization within the dividing NSC is shown below.

277 (B) Quantification of chromosome decompaction, nuclear separation, and nuclear import, relative to
278 cytokinetic pore diameter. Each point represents a distinct NSC division.

279 (C) Nuclear dynamics during late NSC division focusing on the cytokinetic pore and nascent NP sibling.
280 Frames from Video 2 are shown with Klaroid-GFP expressed from its native promoter and the plasma
281 membrane marker PLC δ -PH-mCherry (expressed with worniu-GAL4 driven UAS) through an optical
282 section containing the cytokinetic pore. Arrowheads point to cortical Pros signal in dividing NSC and
283 nascent NP sibling. Time in minutes relative to nuclear membrane separation is shown along with the
284 diameter of the cytokinetic pore in microns. A schematic representation of the nascent siblings is
285 shown below.

286 (D) Nuclear import dynamics during late NSC division focusing on the cytokinetic pore and nascent NP
287 sibling. Frames from Video 2 are shown with PLC δ -PH-GFP and NLS-DsRed (both expressed with
288 Worniu-GAL4 driven UAS) through an optical section containing the cytokinetic pore. Time in minutes
289 relative to nuclear import onset is shown along with the diameter of the cytokinetic pore in microns. A
290 schematic representation of the nascent siblings is shown below.

291 (E) Timeline of late NSC division and initiation of fate determinant activation.

292 Figure 3 Fate determinants are isolated in nascent siblings before abscission

293 (A) Dynamics of the fate determinant Brain tumor (Brat) during the late stages of NSC asymmetric
294 division focusing on the cytokinetic pore and nascent NP sibling. Frames from Video 3 are shown with
295 GFP-Brat expressed from its endogenous locus and the plasma membrane marker PLC δ -PH-mCherry
296 (expressed with Worniu-GAL4 driven UAS) through an optical section containing the cytokinetic pore.
297 Time in minutes relative to Brat translocation from the membrane to the cytoplasm is shown along
298 with the diameter of the cytokinetic pore in microns. A schematic representation of the localization in
299 the dividing NSC is shown below.

300 (B) Quantification of Brat membrane release as a function of cytokinetic pore diameter for three
301 different NSCs.

302 (C) Microtubule dynamics during the late stages of NSC asymmetric division focusing on the cytokinetic
303 pore and nascent NP sibling. Frames from Video 3 are shown with the microtubule marker Jupiter-GFP
304 and the plasma membrane marker PLC δ -PH-mCherry (expressed with Worniu-GAL4 driven UAS). Time
305 in minutes relative to central spindle compaction is shown along with the diameter of the cytokinetic
306 pore in microns. A schematic representation of the localization in the dividing NSC is shown below.

307 (D) Fascetto (Feo; PRC1 homolog) dynamics during the late stages of NSC asymmetric division focusing
308 on the cytokinetic pore and nascent NP sibling. Frames from Video 3 are shown with Feo-GFP and the
309 plasma membrane marker PLC δ -PH-mCherry (expressed with Worniu-GAL4 driven UAS). Time in
310 minutes relative to Brat translocation from the membrane to the cytoplasm is shown along with the
311 diameter of the cytokinetic pore in microns. A schematic representation of the localization in the
312 dividing NSC is shown below.

313 (E) Model for pre-division initiation of asymmetric fate specification. When mitosis is completed the
314 nascent NSC and NP siblings remain connected by the intercellular bridge, which contains the recently-
315 formed midbody. The midbody consists of central spindle microtubules (which extend between the
316 divided nuclei) and other proteins such as Feo. Shortly after mitosis, fate determinants like Brat and
317 Pros are released from the membrane but don't exchange with the other nascent sibling's cytoplasm.
318 Pros is immediately imported into the nucleus of the nascent NP sibling following release.

319 Figure 4 The cytokinetic midbody is required for cytoplasmic isolation during fate determinant
320 activation

321 (A) Membrane and actin dynamics in NSC with the actin cytoskeleton depolymerized by LatA before
322 midbody formation. Frames from Video 4 are shown with GMA-GFP ("Actin") and PLC δ -PH-mCherry
323 (both expressed with Worniu-GAL4 driven UAS). Time in minutes relative to Latrunculin A (LatA)
324 addition is shown along with the diameter of the cytokinetic pore in microns. A schematized
325 representation of the localization within the dividing NSC is shown below.

326 (B) Membrane and actin dynamics in NSC with the actin cytoskeleton depolymerized by LatA after
327 midbody formation. Frames from Video 4 are shown as in (A).

328 (C) Brat dynamics in NSC with the actin cytoskeleton depolymerized by LatA before midbody
329 formation. Frames from Video 4 are shown with Brat-GFP expressed from its endogenous locus and the
330 plasma membrane marker PLC δ -PH-mCherry (expressed with Worniu-GAL4 driven UAS) through an
331 optical section containing the cytokinetic pore. Time in minutes relative to Latrunculin A addition is
332 shown along with the diameter of the cytokinetic pore in microns. Middle row shows inset of the
333 cytokinetic pore and nascent NP sibling. A schematized representation of the localization within the
334 dividing NSC is shown below.

335 (D) Brat dynamics in NSC with midbody disrupted by LatA + Colcemid treatment. Frames from Video 4
336 are shown with Brat-GFP with time in minutes relative to LatA and Colcemid addition shown along with
337 the diameter of the cytokinetic pore in microns. Middle row shows inset of the cytokinetic pore and
338 nascent NP sibling. A schematized representation of the localization within the dividing NSC is shown
339 below.

340 (E) Quantification of the effect of actin and microtubule depolymerization on Brat asymmetry. The
341 ratio of nascent NSC to NP cytoplasmic Brat signal is shown at 2 and 10 minutes after Brat membrane
342 release. Each line represents paired measurements for an individual cell. Bar in the mean difference
343 comparison represents bootstrap 95% confidence interval.

344 Figure 5 Fate determinant membrane release requires midbody formation

345 (A) Fascetto (Feo; aka PRC₁) dynamics in NSC with Aurora B inhibited after midbody formation. Frames
346 from Video 5 are shown with Feo-GFP expressed from the ubiquitin promoter and the plasma
347 membrane marker PLC δ -PH-mCherry (expressed with Worniu-GAL4 driven UAS) through an optical
348 section containing the cytokinetic pore in an NSC with Aurora B inhibited with the inhibitor Binucleine 2
349 immediately after the cytokinetic pore reached 1.5 μ m in diameter. Time in minutes is shown along
350 with the diameter of the cytokinetic pore in microns. Bottom row shows inset of the cytokinetic pore
351 and nascent NP sibling.

352 (B) Feo dynamics in NSC with Aurora B inhibited after midbody formation. Frames from Video 5 are
353 shown as in (A) with Aurora B inhibited with the inhibitor Binucleine 2 immediately before the
354 cytokinetic pore reached 1.5 μ m in diameter.

355 (C) Quantification of Feo in NSCs with Aurora B inhibited before or after midbody formation. Gardner-
356 Altman estimation plot of the ratio of Feo signal in the midbody to that of the cytoplasm is shown for

357 six different NSC divisions with Aurora B inhibited before or after the cytokinetic pore reached 1.5 μm .
358 The error bars represent one standard deviation (gap is mean); the bar in the mean difference
359 comparison represents bootstrap 95% confidence interval.

360 (D) Quantification of nuclear import in NSCs with Aurora B inhibited before midbody formation. The
361 ratio of nuclear:cytoplasmic Nuclear Localization Signal-DsRed (NLS-DsRed) at a pore size of 3 μM to
362 seven minutes afterwards is shown.

363 (E) Prospero (Pros) dynamics in NSC with Aurora B inhibited after midbody formation. Frames from
364 Video 5 are shown with Pros-GFP expressed from its endogenous locus and the plasma membrane
365 marker PLC δ -PH-mCherry (expressed with Worniu-GAL4 driven UAS) through an optical section
366 containing the cytokinetic pore in an NSC with Aurora B inhibited with the inhibitor binucleine
367 immediately after the cytokinetic pore reached 1.5 μm in diameter. Time in minutes is shown along
368 with the diameter of the cytokinetic pore in microns. An inset of the cytokinetic pore and nascent NP
369 sibling is shown. The bottom row is a schematized representation of the localization within the dividing
370 NSC.

371 (F) Pros dynamics in NSC with Aurora B inhibited before midbody formation. Frames from Video 5 are
372 shown as in (E) with Aurora B inhibited with the inhibitor Binucleine 2 immediately before the
373 cytokinetic pore reached 1.5 μm in diameter.

374 (G) Quantification of Pros membrane dynamics in dividing NSCs when Aurora B was inhibited before or
375 after midbody formation. Gardner-Altman estimation plot of the membrane to cytoplasmic Pros signal
376 in the nascent NP when the cytokinetic pore reached 3 μm divided by membrane to cytoplasmic Pros
377 seven minutes afterwards. The error bars represent one standard deviation (gap is mean); the bar in the
378 mean difference comparison represents bootstrap 95% confidence interval.

379 (H) Quantification of Pros nuclear dynamics in dividing NSCs when Aurora B was inhibited before or
380 after midbody formation. The ratio of nuclear to cytoplasmic Pros signal in the nascent NP is shown
381 seven minutes following when the cytokinetic pore reached 3 μm for NSCs with Aurora B inhibited with
382 the inhibitor Binucleine 2 immediately before or after the cytokinetic pore reached 1.5 μm in diameter.
383 The error bar represents one standard deviation (gap is mean).

384 (I) Brain Tumor (Brat) dynamics in NSC with Aurora B inhibited after midbody formation. Frames from
385 Video 5 are shown with Brat-GFP expressed from its endogenous locus and the plasma membrane

386 marker PLC δ -PH-mCherry (expressed with Worniu-GAL4 driven UAS) through an optical section
387 containing the cytokinetic pore in an NSC with Aurora B inhibited with the inhibitor Binucleine 2
388 immediately after the cytokinetic pore reached 1.5 μ m in diameter. Time in minutes is shown along
389 with the diameter of the cytokinetic pore in microns. An inset of the cytokinetic pore and nascent NP
390 sibling is shown. The bottom row is a schematized representation of the localization within the dividing
391 NSC.

392 (J) Brat dynamics in NSC with Aurora B inhibited before midbody formation. Frames from Video 5 are
393 shown as in (I) with Aurora B inhibited with the inhibitor Binucleine 2 immediately before the
394 cytokinetic pore reached 1.5 μ m in diameter.

395 (K) Quantification of Brat membrane dynamics in dividing NSCs when Aurora B was inhibited before or
396 after midbody formation. Gardner-Altman estimation plot of the membrane to cytoplasmic Brat signal
397 in the nascent NP when the cytokinetic pore reached 4 μ m divided by membrane to cytoplasmic Brat
398 seven minutes afterwards. The error bars represent one standard deviation (gap is mean); the bar in the
399 mean difference comparison represents bootstrap 95% confidence interval.

400 Figure 6 The cell cycle phosphatase String (Cdc25) is required for fate determinant membrane release
401 following midbody formation

402 (A) Inhibition of String (Cdc25) leads to delayed Pros release. Frames from Video 6 are shown with Pros-
403 GFP expressed from its endogenous locus and the plasma membrane marker PLC δ -PH-mCherry
404 (expressed with Worniu-GAL4 driven UAS) through an optical section containing the cytokinetic pore in
405 NSCs treated with the String inhibitor. Time in minutes relative to the Pros membrane release is shown
406 along with the diameter of the cytokinetic pore in microns. Merge is shown in the second row along
407 with an inset in the third row that focuses on the cytokinetic pore and NP sibling. Bottom row shows a
408 schematized representation of the localization.

409 (B) Quantification of the effect of String inhibition on Pros membrane release. Gardner-Altman
410 estimation plot of the number of minutes after the cytokinetic pore reached 1.5 μ m that Pros was
411 released from the membrane. The error bars represent one standard deviation (gap is mean); the bar in
412 the mean difference comparison represents bootstrap 95% confidence interval.

413 (C) String localization during late NSC cytokinesis. An NSC expressing PLC δ -PH-GFP (expressed with
414 Worniu-GAL4 driven UAS) fixed and stained with anti-String ("String") and anti-GFP ("membrane")
415 antibodies is shown.

416 **Resource Availability**

417 **Lead Contact**

418 Contact the Lead Contact, Kenneth Prehoda (prehoda@uoregon.edu), for further information or
419 to request resources and reagents.

420 **Materials Availability**

421 No new reagents were generated in this study.

422 **Data and Code Availability**

423 Raw data available from the corresponding author on request.

424 **Experimental Model and Subject Details**

425 **Fly Strains**

426 Tissue specific expression of UAS controlled transgenes in NSCs was achieved using a Worniu-
427 GAL4 driver line. Membrane dynamics were imaged using the membrane markers UAS-PLC δ -
428 PH-GFP and UAS-PLC δ -PH-mCherry, which express the pleckstrin homology domain of human
429 PLC δ tagged with GFP or mCherry, and binds to the plasma membrane lipid phosphoinositide
430 PI(4,5)P₂. F-Actin was visualized using UAS-GMA-GFP, which expresses a GFP tagged actin
431 binding domain of Moesin. The onset of nuclear import at the end of mitosis was monitored
432 using UAS-NLS-DsRed, which is comprised of a DsRed protein containing a nuclear localization
433 signal (NLS) and expressed under the control of UAS.

434 Microtubules were imaged using GFP tagged Jupiter⁴². Fascetto (Feo) was imaged using a GFP
435 tagged Fascetto protein under control of ubiquitin regulatory sequences. GFP tagged Prospero
436 (Pros), Brain Tumor (Brat), and Deadpan (Dpn) proteins were generated by the modERN
437 Project⁴³. The nuclear envelope was imaged using GFP tagged Klaroid⁴⁴. Chromosomes were
438 imaged using RFP tagged Histone 2A (His2a).

439 **Method Details**

440 **Live Imaging**

441 To obtain brain explants, third instar *Drosophila* larvae were dissected in Schneider's Insect
442 Media (SIM) and the central nervous system was isolated. Next, larval brain explants were
443 mounted on sterile poly-D-lysine coated 35mm glass bottom dish (ibidi Cat#81156) containing
444 modified minimal hemolymph-like solution (HL3.1). Then, brain explants were imaged using a
445 Nikon Eclipse Ti-2 Yokogawa CSU-W1 SoRa spinning disk microscope equipped dual

446 Photometrics Prime BSI sCMOS cameras using a 60x H₂O objective. 488 nm light was used to
447 illuminate GFP tagged proteins and 561 nm light was used to illuminate DsRed and mCherry
448 tagged proteins. Super resolution imaging was achieved by using SoRa (super resolution
449 through optical photon reassignment) optics⁴⁵. NSCs were identified by their large size, location
450 in the central nervous system, and the use of NSC specific tissue driver lines. Time lapse
451 imaging of midbody dynamics was achieved by refocusing the imaging plane on the medial
452 plane of the cleavage furrow, and subsequently the midbody, along the apical-basal axis just
453 before capturing each frame. Pharmacological inhibition of Aurora B was performed using 15
454 μ M Binucleine 2 solubilized in DMSO. Pharmacological depolymerization of microtubules was
455 performed using 1 mM Colcemid solubilized in DMSO. Pharmacological depolymerization of F-
456 actin was performed using 50 μ M Latrunculin A (LatA) solubilized in DMSO. Pharmacological
457 inhibition of String was performed using 750 μ M of the Cdc25 inhibitor NSC 663284 solubilized
458 in DMSO.

459 **Immunofluorescence Staining**

460 To determine the localization of native String in NSCs, the central nervous systems of third
461 instar *Drosophila* larvae expressing Worniu-GAL4>UAS-PLC δ -PH-GFP were fixed in 4%
462 paraformaldehyde. Mouse anti-GFP antibodies were used to stain NSC membranes (marked by
463 Worniu-GAL4 driven UAS-PLC δ -PH-GFP), and guinea pig anti-String antibodies were used to
464 stain String. Primary antibodies were used at a concentration of 1:100 (anti-GFP) and 1:75 (anti-
465 String). Alexa 488 labeled anti-mouse (Invitrogen) and Cy3 labeled anti-guinea pig (Jackson
466 Labs) secondary antibodies were used at a concentration of 1:500. Super resolution images
467 were captured using a Nikon Eclipse Ti-2 Yokogawa CSU-W1 SoRa spinning disk microscope
468 equipped dual Photometrics Prime BSI sCMOS cameras using a 60x H₂O objective.

469 **Image Processing and Analysis**

470 Imaging data was processed using ImageJ (FIJI package). For some movies, the bleach
471 correction tool was used to correct for photobleaching. To reduce noise in Deadpan images,
472 Gaussian blur was applied. For quantifying the dynamics of the cytokinetic pore size, medial
473 sections (along the apical-basal axis) were used to measure the width of the cytokinetic pore. If
474 ever the pore moved out of the focal plane, the pore size of the previous frame was used.

475 Quantification for Fig. 1D: The cytokinetic pore diameter was measured at the onset of Prospero
476 membrane release for n=10 dividing NSCs.

477 Quantification for Fig. 1E: To quantify cytokinetic pore closure dynamics, the pore size was
478 measure as a function of time and plotted for n=5 dividing NSCs.

479 Quantification for Fig. 1G: The cytokinetic pore diameter was measured at the onset of Deadpan
480 nuclear import for n=3 dividing NSCs.

481 Quantification for Fig. 2B: The cytokinetic pore diameter was measured at the onset of
482 chromosome decompaction, nuclear separation, and the onset of nuclear import. His2a-RFP
483 signal was used to determine when chromosome began to decompact for n=3 dividing NSCs.
484 Klaroid-GFP was used to determine when the nascent sibling nuclear compartments became
485 separated for n=3 dividing NSCs. NLS-DsRed was used to determine the onset of nuclear
486 import for n=3 dividing NSCs. Nuclear import was determined by the frame in which nuclear
487 intensity of NLS-DsRed began to increase.

488 Quantification for Fig. 3B: To quantify the timing of Brat membrane release during NSC division,
489 Image J was used to measure average cytoplasmic signal intensity in the nascent NP and
490 nascent NSC sibling cytoplasm. The ratio of nascent NP:NSC cytoplasmic Brat signal was
491 plotted as a function of cytokinetic pore constriction.

492 Quantification for Fig. 4E: To quantify the effect of actin and microtubule depolymerization on
493 Brat asymmetry, Brat signal in the nascent NSC and NP cytoplasm was measured to calculate
494 the nascent NP:NSC cytoplasmic Brat ratio. This ratio was calculated at 2 and 10 minutes after
495 Brat membrane release was detected. Latrunculin A treated dividing NSCs (n=3) were
496 compared to Latrunculin A + Colcemid treated dividing NSCs (n=3).

497 Quantification for Fig. 5C: To quantify the effect of Aurora B inhibition on Fascetto dynamics,
498 Fascetto signal intensity within the midbody and within the nascent NSC cytoplasm was
499 measured to calculate a midbody:cytoplasmic ratio. Measurements were taken when the
500 cytokinetic pore constricted to under 3 μm . Using Image J, average signal intensity within a 3
501 μm x 3 μm box drawn over the midbody was used to measure Fascetto signal intensity in the
502 midbody. The same size box was used to measure average Fascetto signal intensity within the
503 nascent NSC cytoplasm adjacent to the midbody. Dividing NSCs where Aurora B inhibition
504 occurred after midbody formation (n=6) were compared to dividing NSCs where Aurora B
505 inhibition occurred before midbody formation (n=6).

506 Quantification for Fig. 5D: To determine the effect of Aurora B inhibition on nuclear import
507 dynamics, nuclear:cytoplasmic ratio of the nuclear marker NLS-DsRed was calculated for
508 dividing NSCs where Aurora B inhibition occurred before midbody formation. Average signal
509 intensity of NLS-DsRed within the nuclear compartment and within the cytoplasm was
510 measured to calculate a nuclear:cytoplasm ratio for n=3 dividing NSCs.

511 Quantification for Fig. 5G: To quantify the effect of Aurora B inhibition on Prospero dynamics,
512 Prospero signal intensity on the nascent NP membrane and within the nascent NP cytoplasm
513 was measured to calculate a membrane:cytoplasm ratio. Using Image J, Prospero membrane
514 intensity was measured by tracing the plasma membrane (marked by UAS-PLC δ -PH-mCherry)
515 and then copying the ROI (region of interest) to the Prospero channel. A line of similar length
516 was drawn within the nascent NP cytoplasm. Measurements were taken when the cytokinetic
517 pore constricted to under 3 μm and then again 7 minutes later. Dividing NSCs where Aurora B
518 inhibition occurred after midbody formation (n=6) were compared to dividing NSCs where
519 Aurora B inhibition occurred before midbody formation (n=6).

520 Quantification for Fig. 5H: Nuclear Prospero signal intensity was measured by outlining the
521 nascent NP nucleus and measuring average signal intensity within. Nuclear:cytoplasm ratios
522 were calculated 7 minutes after the pore has constricted down to 3 μm . Dividing NSCs where
523 Aurora B inhibition occurred after midbody formation (n=6) were compared to dividing NSCs
524 where Aurora B inhibition occurred before midbody formation (n=6).

525 Quantification for Fig. 5K: To quantify the effect of Aurora B inhibition on Brat dynamics, Brat
526 signal intensity on the nascent NP membrane and within the nascent NP cytoplasm was
527 measured to calculate a membrane:cytoplasm ratio. Using Image J, Brat membrane intensity
528 was measured by tracing the plasma membrane (marked by UAS-PLC δ -PH-mCherry) and then
529 copying the ROI (region of interest) to the Brat channel. A line of similar length was drawn within
530 the nascent NP cytoplasm. Measurements were taken when the cytokinetic pore constricted to
531 under 4 μm and then again 7 minutes later. Dividing NSCs where Aurora B inhibition occurred

532 after midbody formation (n=6) were compared to dividing NSCs where Aurora B inhibition
533 occurred before midbody formation (n=6).

534 Quantification for Fig. 6B: The effect of String inhibition on Prospero dynamics was measured
535 by, waiting until the cytokinetic pore constricted to 1.5 μ m and then determining the time until
536 onset Prospero nuclear import into the nascent NP nucleus. Dividing NSCs treated with the
537 String inhibitor NSC 663284 (n=3) were compared to DMSO alone (n=3).

538 **Statistical Analysis**

539 Gardner-Altman estimation plots and 95% confidence intervals of datasets were prepared using
540 the DABEST package⁴⁶. Statistical details can be found in the relevant methods section and
541 figure legend

542 **Key Resources Table**

REAGENT or RESOURCE	SOURCE	IDENTIFIER
Experimental Model: Fly Strains		
Brain Tumor (Brat)-GFP	Bloomington <i>Drosophila</i> Stock Center (BDSC)	BDSC Cat#83658 RRID: BDSC 83658
Deadpan (Dpn)-GFP	Bloomington <i>Drosophila</i> Stock Center (BDSC)	BDSC Cat#65295 RRID: BDSC 65295
Fascetto (Feo)-GFP	Bloomington <i>Drosophila</i> Stock Center (BDSC)	BDSC Cat#59273 RRID: BDSC 59273
His2a-RFP (chromosome marker)	Bloomington <i>Drosophila</i> Stock Center (BDSC)	BDSC Cat# 23650 RRID: BDSC 23650
Jupiter-GFP (microtubule marker)	Bloomington <i>Drosophila</i> Stock Center (BDSC)	BDSC Cat#60156 RRID: BDSC 60156
Klaroid-GFP (nuclear envelope marker)	Bloomington <i>Drosophila</i> Stock Center (BDSC)	BDSC Cat#51525 RRID: BDSC 51525
Prospero (Pros)-GFP	Bloomington <i>Drosophila</i> Stock Center (BDSC)	BDSC Cat#66463 RRID: BDSC 66463
UAS-GMA-GFP (F-actin marker)	Bloomington <i>Drosophila</i> Stock Center (BDSC)	BDSC Cat#31776 RRID: BDSC 31776
UAS-PLC δ -PH-GFP (membrane marker)	Bloomington <i>Drosophila</i> Stock Center (BDSC)	BDSC Cat#39693 RRID: BDSC 39693
UAS-PLC δ -PH-mCherry (membrane marker)	Bloomington <i>Drosophila</i> Stock Center (BDSC)	BDSC Cat#51658 RRID: BDSC 51658
UAS-NLS-DsRed (nuclear marker)	Bloomington <i>Drosophila</i> Stock Center (BDSC)	BDSC Cat#8547 RRID: BDSC 8547
Worniu-GAL4 (NSC driver line)	Chris Q. Doe Lab	
Pharmacological Inhibitors		
Binucleine 2	Sigma-Aldrich	Cat#B1186
Colcemid	Millipore	Cat#234109-M
Latrunculin A (LatA)	Enzo	Cat#BML-T119-0100
NSC 663284	Cayman Chemical	Cat#13303
Primary Antibodies		
anti-GFP	Developmental Studies	Cat# DSHB-GFP-12A6

	Hybridoma Bank	RRID: AB_2617417
anti-String	Yukiko M. Yamashita Lab	

543

544 **Video Legends**

545 **Video 1: Asymmetric fate specification is initiated before NSC division completes**

546 Part 1: Prospero dynamics during the late stages of NSC asymmetric division. Super resolution
547 videos of NSCs expressing Prospero-GFP “Prospero” and the membrane marker UAS-PLCδ-
548 PH-mCherry “membrane”. Time relative to start of nuclear import of Prospero is indicated. Three
549 movies of dividing NSCs are shown.

550 Part 2: Deadpan dynamics during the late stages of NSC asymmetric division. Super resolution
551 videos of NSCs expressing Deadpan-GFP “Deadpan” and the membrane marker UAS-PLCδ-
552 PH-mCherry “membrane”. To improve image quality, Gaussian blur was applied to the Deadpan
553 channel. Time relative to start of nuclear import of Deadpan is indicated. Three movies of
554 dividing NSCs are shown.

555 **Video 2: A temporal window between mitosis and cytokinesis during NSC asymmetric cell division**

557 Part 1: Chromatin dynamics during late NSC division. Super resolution videos of NSCs
558 expressing the chromosome marker His2a-RFP “His2a” and the membrane marker UAS-PLCδ-
559 PH-GFP “membrane”. Time relative to start of chromosome decompaction is indicated. Three
560 movies of dividing NSCs are shown.

561 Part 2: Nuclear dynamics during late NSC division. Super resolution videos of NSCs expressing
562 the nuclear envelope marker Klaroid-GFP “Klaroid” and the membrane marker UAS-PLCδ-PH-
563 mCherry “membrane”. Time relative to nuclear membrane separation. Three movies of dividing
564 NSCs are shown.

565 Part 3: Nuclear import dynamics during late NSC division. Super resolution videos of NSCs
566 expressing the nuclear marker UAS-NLS-DsRed “NLS-DsRed” and the membrane marker UAS-
567 PLCδ-PH-GFP “membrane”. Time relative to start of nuclear import is indicated. Three movies
568 of dividing NSCs are shown.

569 **Video 3: Fate determinants are isolated in nascent siblings before NSC division completes**

571 Part 1: Brat dynamics during late NSC division. Super resolution videos of NSCs expressing
572 Brain Tumor (Brat)-GFP “Brat” and the membrane marker UAS-PLCδ-PH-mCherry
573 “membrane”. Time relative to membrane release of Brat. Three movies of dividing NSCs are
574 shown.

575 Part 2: Microtubule dynamics during late NSC division. Super resolution videos of NSCs
576 expressing the microtubule marker Jupiter-GFP “microtubules” and the membrane marker UAS-
577 PLCδ-PH-mCherry “membrane”. Bottom row is a zoomed-in view of the cytokinetic pore. Time
578 relative to midbody formation. Three movies of dividing NSCs are shown.

579 Part 3: Fascetto dynamics during late NSC division. Super resolution videos of NSCs
580 expressing Fascetto-GFP “Fascetto” and the membrane marker UAS-PLCδ-PH-mCherry
581 “membrane”. Bottom row is a zoomed-in view of the cytokinetic pore. Time relative to midbody
582 formation. Three movies of dividing NSCs are shown.

583 **Video 4: The cytokinetic midbody is required for cytoplasmic isolation during fate**
584 **determinant activation**

585 Part 1: Membrane and actin dynamics in NSC with the actin cytoskeleton depolymerized by
586 LatA before midbody formation. Super resolution videos of NSCs expressing the F-actin marker
587 UAS-GMA-GFP “F-actin” and the membrane marker UAS-PLCδ-PH-mCherry “membrane” in
588 the presence of the F-actin inhibitor, Latrunculin A (LatA). Bottom row is a zoomed-in view of the
589 cytokinetic pore. Time relative to LatA addition.

590 Part 2: Membrane and actin dynamics in NSC with the actin cytoskeleton depolymerized by
591 LatA after midbody formation. Super resolution videos of NSCs expressing the F-actin marker
592 UAS-GMA-GFP “F-actin” and the membrane marker UAS-PLCδ-PH-mCherry “membrane” in
593 the presence of the F-actin inhibitor, Latrunculin A (LatA). Bottom row is a zoomed-in view of the
594 cytokinetic pore. Time relative to LatA addition.

595 Part 3: Brat dynamics in NSCs with the actin cytoskeleton depolymerized by LatA after midbody
596 formation. Super resolution videos of NSCs expressing Brain Tumor (Brat)-GFP “Brat” and the
597 membrane marker UAS-PLCδ-PH-mCherry “membrane” in the presence of the F-actin inhibitor,
598 Latrunculin A (LatA). The drug was added just after midbody formation. Time relative to
599 membrane release of Brat. Three movies of dividing NSCs are shown.

600 Part 4: Brat dynamics in NSC with midbody disrupted by LatA + Colcemid treatment. Super
601 resolution videos of NSCs expressing Brain Tumor (Brat)-GFP “Brat” and the membrane marker
602 UAS-PLCδ-PH-mCherry “membrane” in the presence of the F-actin inhibitor, Latrunculin A
603 (LatA), and the microtubule inhibitor, Colcemid. The drug cocktail was added just after midbody
604 formation. Time relative to membrane release of Brat. Three movies of dividing NSCs are
605 shown.

606 **Video 5: Fate determinant membrane release requires midbody formation**

607 Part 1: Fascetto dynamics in NSCs with Aurora B inhibited before midbody formation. Super
608 resolution videos of NSCs expressing Fascetto-GFP “Fascetto” and the membrane marker
609 UAS-PLCδ-PH-mCherry “membrane” in the presence of the Aurora B inhibitor, Binucleine 2.
610 Time relative to start of imaging. Six movies of dividing NSCs are shown.

611 Part 2: Fascetto dynamics in NSCs with Aurora B inhibited after midbody formation. Super
612 resolution videos of NSCs expressing Fascetto-GFP “Fascetto” and the membrane marker
613 UAS-PLCδ-PH-mCherry “membrane” in the presence of the Aurora B inhibitor, Binucleine 2.
614 Time relative to start of imaging. Six movies of dividing NSCs are shown.

615 Part 3: Prospero dynamics in NSCs with Aurora B inhibited before midbody formation. Super
616 resolution videos of NSCs expressing Prospero-GFP “Prospero” and the membrane marker
617 UAS-PLCδ-PH-mCherry “membrane” in the presence of the Aurora B inhibitor, Binucleine 2.
618 Time relative to start of imaging. Six movies of dividing NSCs are shown.

619 Part 4: Prospero dynamics in NSCs with Aurora B inhibited after midbody formation. Super
620 resolution videos of NSCs expressing Prospero-GFP “Prospero” and the membrane marker
621 UAS-PLCδ-PH-mCherry “membrane” in the presence of the Aurora B inhibitor, Binucleine
622 2Time relative to start of imaging. Six movies of dividing NSCs are shown.

623 Part 5: Brat dynamics in NSCs with Aurora B inhibited before midbody formation. Super
624 resolution videos of NSCs expressing Brain Tumor (Brat)-GFP “Brat” and the membrane marker
625 UAS-PLCδ-PH-mCherry “membrane” in the presence of the Aurora B inhibitor, Binucleine 2.
626 Time relative to start of imaging. Six movies of dividing NSCs are shown.

627 Part 6: Brat dynamics in NSCs with Aurora B inhibited after midbody formation. Super resolution
628 videos of NSCs expressing Brain Tumor (Brat)-GFP “Brat” and the membrane marker UAS-
629 PLCδ-PH-mCherry “membrane” in the presence of the Aurora B inhibitor, Binucleine 2. Time
630 relative to start of imaging. Six movies of dividing NSCs are shown.

631 Part 7: Nuclear import dynamics in NSCs with Aurora B inhibited before midbody formation.
632 Super resolution videos of NSCs expressing the nuclear marker UAS-NLS-DsRed “NLS-DsRed”
633 and the membrane marker UAS-PLCδ-PH-GFP “membrane in the presence of the Aurora B
634 inhibitor, Binucleine 2. Time relative to start of imaging. Three movies of dividing NSCs are
635 shown.

636 **Video 6: The cell cycle phosphatase String (Cdc25) is required for fate determinant** 637 **membrane release following midbody formation**

638 Part 1: Prospero dynamics with String (Cdc25) inhibited. Super resolution videos of NSCs
639 expressing Prospero-GFP “Prospero” and the membrane marker UAS-PLCδ-PH-mCherry
640 “membrane” in the presence of the String inhibitor, NSC 663284. The drug was added just prior
641 to midbody formation. Time relative to start of nuclear import of Prospero is indicated. Three
642 movies of dividing NSCs are shown.

643 Part 2: Prospero dynamics in NSCs treated with DMSO (vehicle control). Prospero-GFP
644 “Prospero” and the membrane marker UAS-PLCδ-PH-mCherry “membrane” in the presence of
645 2% DMSO. The DMSO was added just prior to midbody formation. Time relative to start of
646 nuclear import of Prospero is indicated. Three movies of dividing NSCs are shown.

647 **Acknowledgments**

648 We thank Brad Nolen and Daniel Grimes for their useful comments on this manuscript. We
649 thank Adam Fries for maintaining the microscope used in this study. We thank Yukiko
650 Yamashita for the anti-String antibody. This work was supported by NIH grants R35GM127092
651 and K99GM147601.

652 **Author Contributions**

653 B.L. and K.E.P. designed the experiments. B.L. performed the experiments. R.R.P. contributed
654 to the String inhibition and String staining experiments. B.L. and K.E.P analyzed the data,
655 prepared the figures, and wrote the manuscript.

656 **Declaration of Interests**

657 The authors have no competing interests to declare.

658

659 References

- 660 1. Horvitz, H. R. & Herskowitz, I. Mechanisms of asymmetric cell division: two Bs or not two Bs, that is the
661 question. *Cell* **68**, 237–255 (1992).
- 662 2. Sunchu, B. & Cabernard, C. Principles and mechanisms of asymmetric cell division. *Dev. Camb. Engl.* **147**,
663 dev167650 (2020).
- 664 3. Knoblich, J. A. Asymmetric cell division during animal development. *Nat. Rev. Mol. Cell Biol.* **2**, 11–20 (2001).
- 665 4. Venkei, Z. G. & Yamashita, Y. M. Emerging mechanisms of asymmetric stem cell division. *J. Cell Biol.* (2018)
666 doi:10.1083/jcb.201807037.
- 667 5. Gönczy, P. Mechanisms of asymmetric cell division: flies and worms pave the way. *Nat. Rev. Mol. Cell Biol.* **9**,
668 355–366 (2008).
- 669 6. Williams, S. E. & Fuchs, E. Oriented divisions, fate decisions. *Curr. Opin. Cell Biol.* **25**, 749–758 (2013).
- 670 7. Knoblich, J. A. Asymmetric cell division: recent developments and their implications for tumour biology. *Nat.*
671 *Rev. Mol. Cell Biol.* **11**, 849–860 (2010).
- 672 8. Knoblich, J. A., Jan, L. Y. & Jan, Y. N. Asymmetric segregation of Numb and Prospero during cell division.
673 *Nature* **377**, 624–627 (1995).
- 674 9. Hirata, J., Nakagoshi, H., Nabeshima, Y. & Matsuzaki, F. Asymmetric segregation of the homeodomain protein
675 Prospero during *Drosophila* development. *Nature* **377**, 627–630 (1995).
- 676 10. Doe, C. Q., Chu-LaGraff, Q., Wright, D. M. & Scott, M. P. The prospero gene specifies cell fates in the
677 *Drosophila* central nervous system. *Cell* **65**, 451–464 (1991).
- 678 11. Choksi, S. P. *et al.* Prospero acts as a binary switch between self-renewal and differentiation in *Drosophila*
679 neural stem cells. *Dev. Cell* **11**, 775–789 (2006).
- 680 12. Chaigne, A. *et al.* Abscission Couples Cell Division to Embryonic Stem Cell Fate. *Dev. Cell* **55**, 195–208.e5
681 (2020).
- 682 13. Egli, D., Birkhoff, G. & Eggan, K. Mediators of reprogramming: transcription factors and transitions through
683 mitosis. *Nat. Rev. Mol. Cell Biol.* **9**, 505–516 (2008).
- 684 14. Dalton, S. Linking the Cell Cycle to Cell Fate Decisions. *Trends Cell Biol.* **25**, 592–600 (2015).

- 685 15. Boward, B., Wu, T. & Dalton, S. Concise Review: Control of Cell Fate Through Cell Cycle and Pluripotency
686 Networks. *Stem Cells Dayt. Ohio* **34**, 1427–1436 (2016).
- 687 16. Soufi, A. & Dalton, S. Cycling through developmental decisions: how cell cycle dynamics control pluripotency,
688 differentiation and reprogramming. *Dev. Camb. Engl.* **143**, 4301–4311 (2016).
- 689 17. Pelham-Webb, B., Murphy, D. & Apostolou, E. Dynamic 3D Chromatin Reorganization during Establishment
690 and Maintenance of Pluripotency. *Stem Cell Rep.* **15**, 1176–1195 (2020).
- 691 18. Palozola, K. C. *et al.* Mitotic transcription and waves of gene reactivation during mitotic exit. *Science* **358**, 119–
692 122 (2017).
- 693 19. Andrade, V. & Echard, A. Mechanics and regulation of cytokinetic abscission. *Front. Cell Dev. Biol.* **10**, 1046617
694 (2022).
- 695 20. Gershony, O., Pe'er, T., Noach-Hirsh, M., Elia, N. & Tzur, A. Cytokinetic abscission is an acute G1 event. *Cell*
696 *Cycle Georget. Tex* **13**, 3436–3441 (2014).
- 697 21. Nähse, V., Christ, L., Stenmark, H. & Campsteijn, C. The Abscission Checkpoint: Making It to the Final Cut.
698 *Trends Cell Biol.* **27**, 1–11 (2017).
- 699 22. Roubinet, C., White, I. J. & Baum, B. Asymmetric nuclear division in neural stem cells generates sibling nuclei
700 that differ in size, envelope composition, and chromatin organization. *Curr. Biol. CB* **31**, 3973–3983.e4 (2021).
- 701 23. Roth, M., Roubinet, C., Iffländer, N., Ferrand, A. & Cabernard, C. Asymmetrically dividing Drosophila
702 neuroblasts utilize two spatially and temporally independent cytokinesis pathways. *Nat. Commun.* **6**, 6551
703 (2015).
- 704 24. Guizetti, J. *et al.* Cortical constriction during abscission involves helices of ESCRT-III-dependent filaments.
705 *Science* **331**, 1616–1620 (2011).
- 706 25. Loyer, N. & Januschke, J. The last-born daughter cell contributes to division orientation of Drosophila larval
707 neuroblasts. *Nat. Commun.* **9**, 3745 (2018).
- 708 26. Bier, E., Vaessin, H., Younger-Shepherd, S., Jan, L. Y. & Jan, Y. N. deadpan, an essential pan-neural gene in
709 Drosophila, encodes a helix-loop-helix protein similar to the hairy gene product. *Genes Dev.* **6**, 2137–2151
710 (1992).

- 711 27. Boettcher, B., Marquez-Lago, T. T., Bayer, M., Weiss, E. L. & Barral, Y. Nuclear envelope morphology
712 constrains diffusion and promotes asymmetric protein segregation in closed mitosis. *J. Cell Biol.* **197**, 921–937
713 (2012).
- 714 28. Shcheprova, Z., Baldi, S., Frei, S. B., Gonnet, G. & Barral, Y. A mechanism for asymmetric segregation of age
715 during yeast budding. *Nature* **454**, 728–734 (2008).
- 716 29. Lee, C.-Y., Wilkinson, B. D., Siegrist, S. E., Wharton, R. P. & Doe, C. Q. Brat is a Miranda cargo protein that
717 promotes neuronal differentiation and inhibits neuroblast self-renewal. *Dev. Cell* **10**, 441–449 (2006).
- 718 30. Bowman, S. K. *et al.* The tumor suppressors Brat and Numb regulate transit-amplifying neuroblast lineages in
719 *Drosophila*. *Dev. Cell* **14**, 535–546 (2008).
- 720 31. Mierzwa, B. & Gerlich, D. W. Cytokinetic abscission: molecular mechanisms and temporal control. *Dev. Cell* **31**,
721 525–538 (2014).
- 722 32. Green, R. A. *et al.* The midbody ring scaffolds the abscission machinery in the absence of midbody
723 microtubules. *J. Cell Biol.* **203**, 505–520 (2013).
- 724 33. Echard, A., Hickson, G. R. X., Foley, E. & O’Farrell, P. H. Terminal cytokinesis events uncovered after an RNAi
725 screen. *Curr. Biol. CB* **14**, 1685–1693 (2004).
- 726 34. Hu, C.-K., Coughlin, M., Field, C. M. & Mitchison, T. J. KIF4 regulates midzone length during cytokinesis. *Curr.*
727 *Biol. CB* **21**, 815–824 (2011).
- 728 35. Hu, C.-K., Coughlin, M. & Mitchison, T. J. Midbody assembly and its regulation during cytokinesis. *Mol. Biol.*
729 *Cell* **23**, 1024–1034 (2012).
- 730 36. Nunes Bastos, R. *et al.* Aurora B suppresses microtubule dynamics and limits central spindle size by locally
731 activating KIF4A. *J. Cell Biol.* **202**, 605–621 (2013).
- 732 37. Smurnyy, Y., Toms, A. V., Hickson, G. R., Eck, M. J. & Eggert, U. S. Binucleine 2, an isoform-specific inhibitor of
733 *Drosophila* Aurora B kinase, provides insights into the mechanism of cytokinesis. *ACS Chem. Biol.* **5**, 1015–1020
734 (2010).
- 735 38. Paweletz, N. Walther Flemming: pioneer of mitosis research. *Nat. Rev. Mol. Cell Biol.* **2**, 72–75 (2001).
- 736 39. Adar-Levor, S. *et al.* Cytokinetic abscission is part of the midblastula transition in early zebrafish
737 embryogenesis. *Proc. Natl. Acad. Sci. U. S. A.* **118**, e2021210118 (2021).

- 738 40. Schulze, E. S. & Blose, S. H. Passage of molecules across the intercellular bridge between post-mitotic
739 daughter cells. *Exp. Cell Res.* **151**, 367–373 (1984).
- 740 41. Jung, G. I. *et al.* An oocyte meiotic midbody cap is required for developmental competence in mice. *Nat.*
741 *Commun.* **14**, 7419 (2023).
- 742 42. Nagarkar-Jaiswal, S. *et al.* A library of MiMICs allows tagging of genes and reversible, spatial and temporal
743 knockdown of proteins in *Drosophila*. *eLife* **2015**, 1–28 (2015).
- 744 43. Kudron, M. M. *et al.* The modern resource: genome-wide binding profiles for hundreds of *Drosophila* and
745 *Caenorhabditis elegans* transcription factors. *Genetics* **208**, 937–949 (2018).
- 746 44. Buszczak, M. *et al.* The carnegie protein trap library: A versatile tool for *drosophila* developmental studies.
747 *Genetics* **175**, 1505–1531 (2007).
- 748 45. Azuma, T. & Kei, T. Super-resolution spinning-disk confocal microscopy using optical photon reassignment.
749 *Opt. Express* **23**, 15003 (2015).
- 750 46. Ho, J., Tumkaya, T., Aryal, S., Choi, H. & Claridge-Chang, A. Moving beyond P values: data analysis with
751 estimation graphics. *Nat. Methods* **16**, 565–566 (2019).
- 752

Figure 1

LaFoya et al.

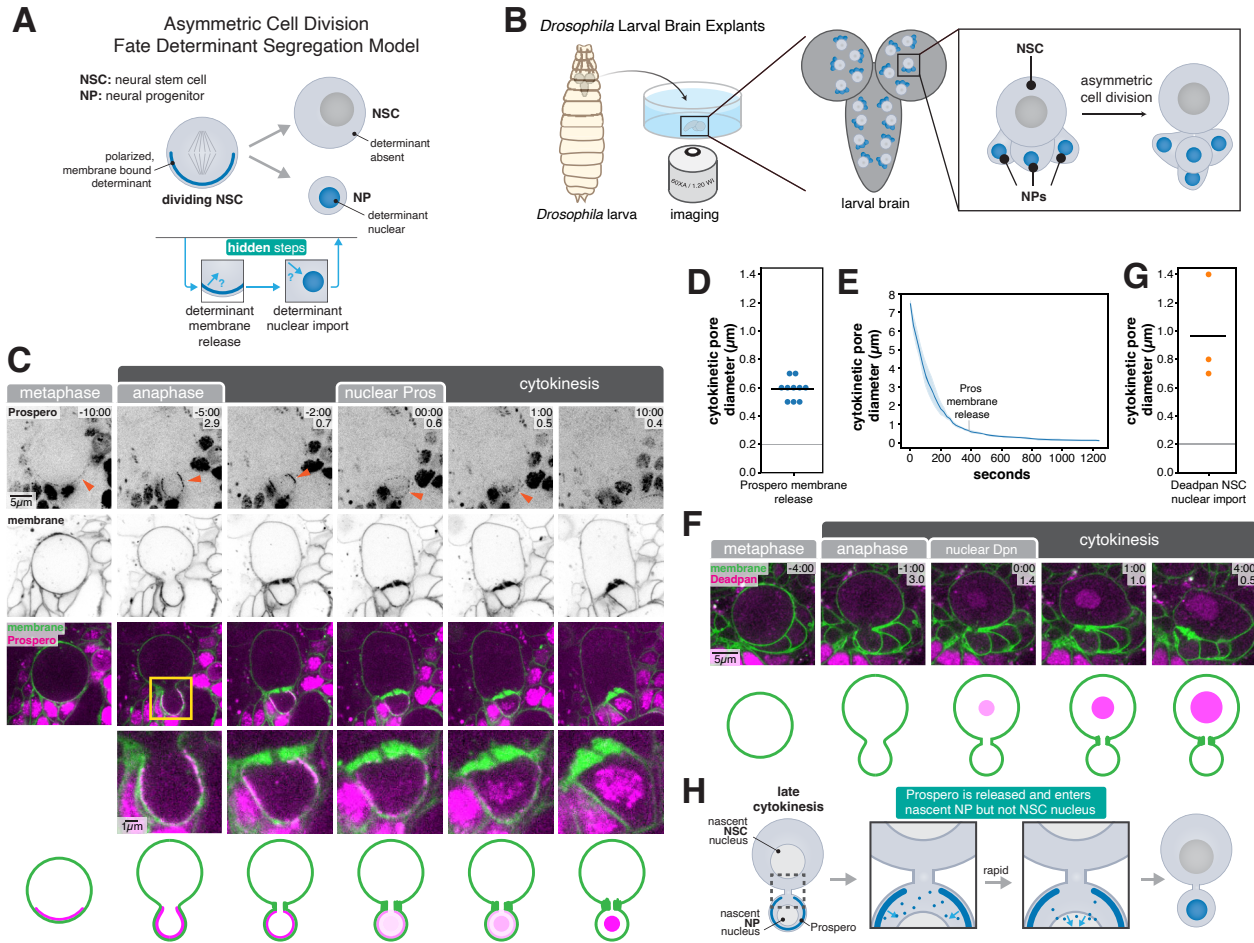


Figure 2

LaFoya et al.

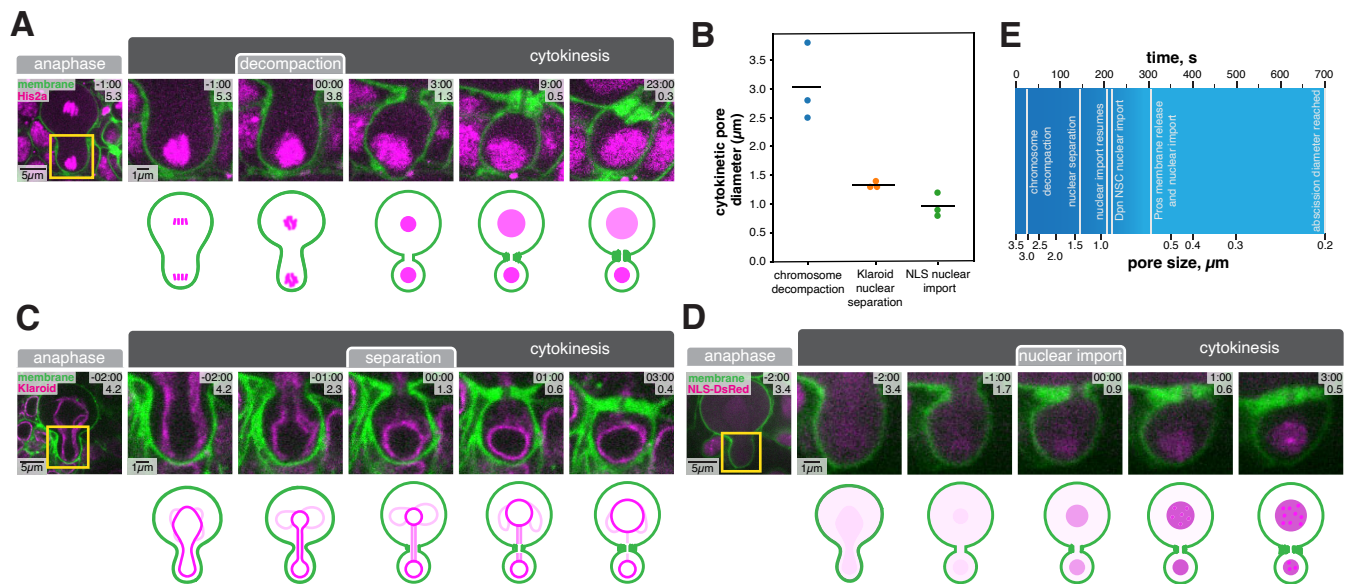


Figure 3

LaFoya et al.

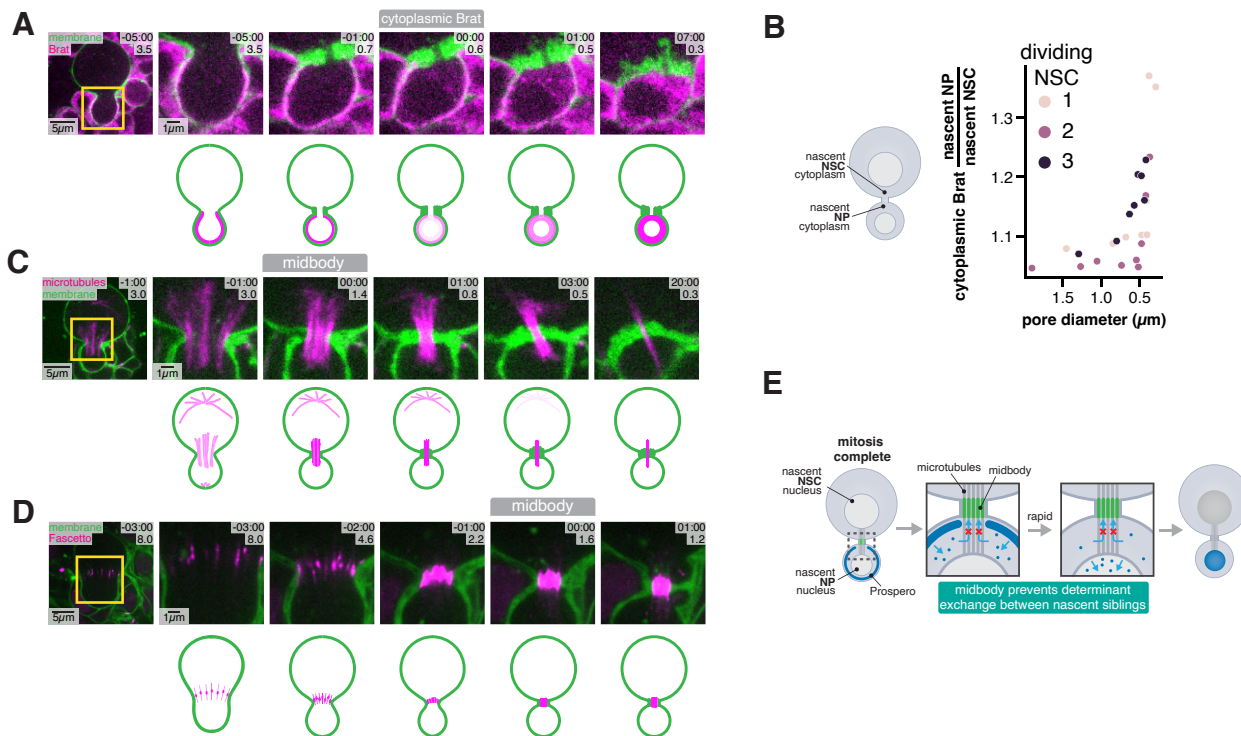


Figure 4

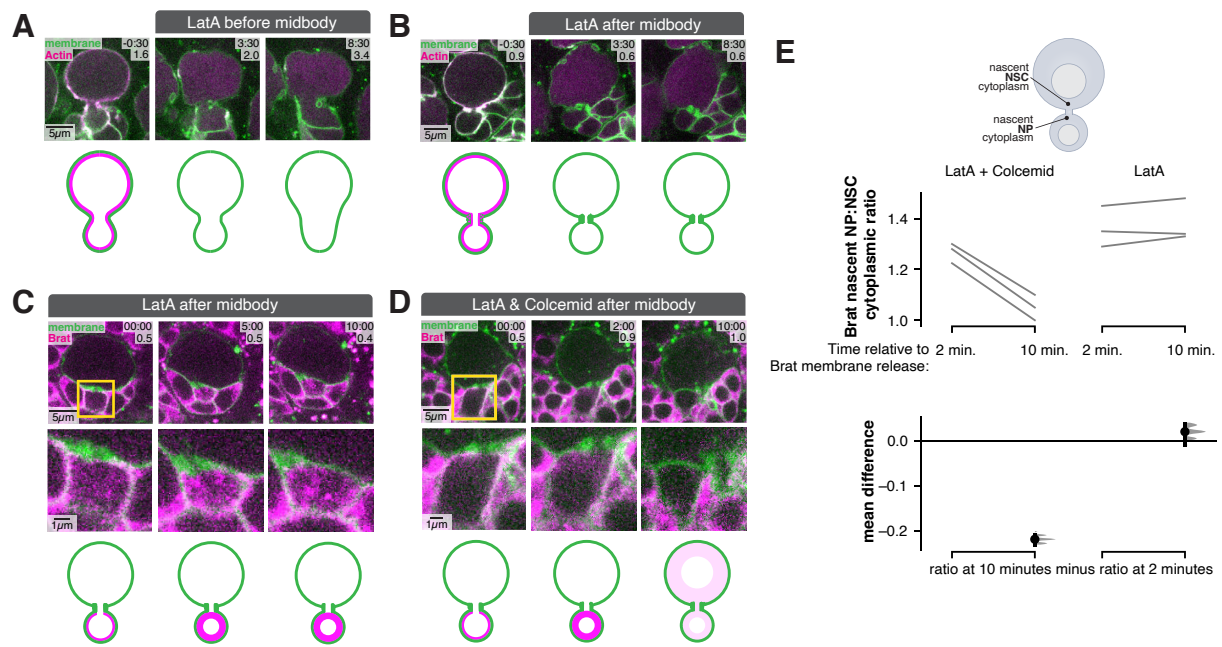


Figure 5

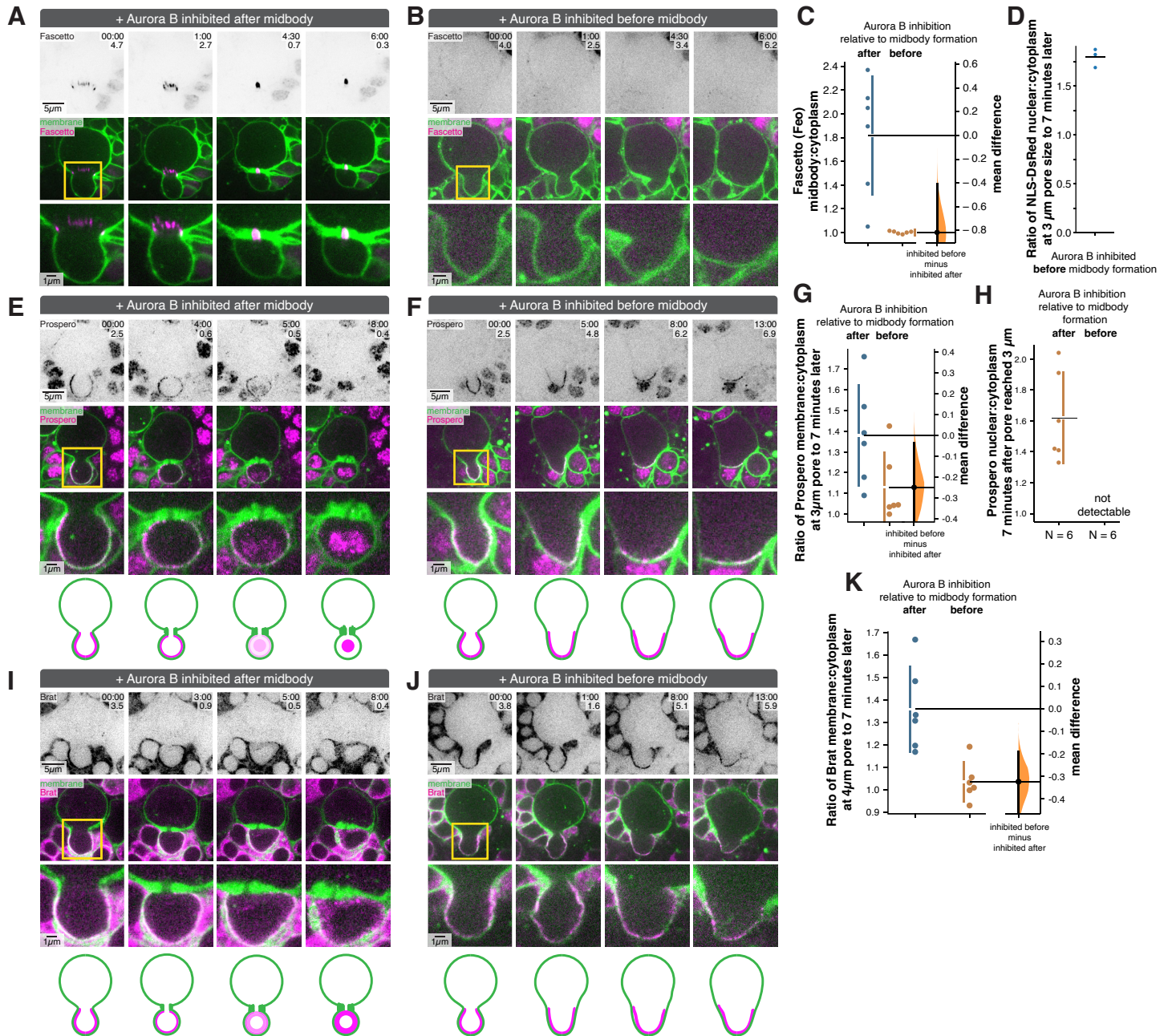


Figure 6

LaFoya et al.

